The Impact of Signal Processing on the Range-Weighting Function for Weather Radars

SEBASTIÁN M. TORRES AND CHRISTOPHER D. CURTIS

Cooperative Institute for Mesoscale Meteorological Studies, University of Oklahoma, and NOAA/OAR/National Severe Storms Laboratory, Norman, Oklahoma

(Manuscript received 18 August 2011, in final form 13 January 2012)

ABSTRACT

The range-weighting function (RWF) determines how individual scatterer contributions are weighted as a function of range to produce the meteorological data associated with a single resolution volume. The RWF is commonly defined in terms of the transmitter pulse envelope and the receiver filter impulse response, and it determines the radar range resolution. However, the effective RWF also depends on the range-time processing involved in producing estimates of meteorological variables. This is a third contributor to the RWF that has become more significant in recent years as advanced range-time processing techniques have become feasible for real-time implementation on modern radar systems. In this work, a new formulation of the RWF for weather radars that incorporates the impact of signal processing is proposed. Following the derivation based on a general signal processing model, typical scenarios are used to illustrate the variety of RWFs that can result from different range-time signal processing techniques. Finally, the RWF is used to measure range resolution and the range correlation of meteorological data.

1. Introduction

The range-weighting function (RWF) is normally introduced in discussions of the radar resolution volume because it defines the radial extent of such volumes. The RWF determines how individual scatterer contributions are weighted as a function of range to produce estimates of the meteorological variables (e.g., reflectivity, Doppler velocity, and the polarimetric variables) associated with a single resolution volume. The RWF is commonly defined in terms of the transmitter pulse envelope and the receiver filter impulse response (section 4.4.2 in Doviak and Zrnić 1993; section 5.3 in Bringi and Chandrasekar 2001) and determines the range resolution of a radar. This form of the RWF is also used for high-resolution radar simulators because it includes the contributing factors before digital sampling occurs (Capsoni and D'Amico 1998; Cheong et al. 2004, 2008). The effective RWF also depends on the digital signal processing of echo samples along the range-time dimension (herein referred to as range-time processing). This third contributor to the RWF has become more significant as novel range-time processing techniques (e.g., those that operate on range-oversampled signals) have become feasible for real-time implementation on modern radar systems. The impact of range-time processing on the RWF is the focus of this paper.

One example of range-time processing that can affect the RWF is range oversampling followed by a whitening transformation (WT; Torres and Zrnić 2003). Range oversampling has been proposed as an effective way to reduce the variance of meteorological variable estimates and/or reduce the required observation times (dwell times) without significantly compromising range resolution. When using a whitening transformation, the time series data are transformed along the range-time dimension. This transformation of the data changes the RWF by combining the range-time samples in a different way compared to a traditional matched filter. Methods for calculating the RWF that were originally developed to study changes in the RWF produced by a whitening transformation are general enough to be applied to a wide variety of range-time processing techniques: from a simple averaging of meteorological variable estimates at contiguous range locations to more recent developments, such as adaptive range oversampling (Curtis and Torres

Corresponding author address: Sebastián Torres, 120 David L. Boren Blvd., National Weather Center, Norman, OK 73072.
E-mail: sebastian.torres@noaa.gov

DOI: 10.1175/JTECH-D-11-00135.1

2011). In this work, the effects of different types of range-time processing on the RWF are examined using typical processing schemes.

The relationship between the RWF and range resolution has already been mentioned, but the RWF is important for several other reasons. Reflectivity gradients can cause biases in reflectivity estimates and can also shift the range location assigned to these data (Mueller 1977; Johnston et al. 2002). Additionally, the combination of the RWF and the resolution volume spacing determines the correlation between the meteorological data in range. This range correlation affects the variance reduction when meteorological variable estimates are averaged along range to gain data precision at the cost of reduced range resolution. Finally, the RWF can also affect the performance of algorithms that process meteorological data. For example, changes in the effective resolution volume in angular and/or range extents can affect tornado detection algorithms that utilize Doppler velocity signatures (Wood and Brown 1997; Torres and Curtis 2006). These effects can be further complicated by the fact that some range-time processing techniques produce a different RWF at each resolution volume. An example is adaptive pseudowhitening; it uses a different linear transformation based on measurements of signal characteristics [e.g., signal-to-noise ratio (SNR) and spectrum width] at every resolution volume (Curtis and Torres 2011). Because of these significant effects, it is important to understand how range-time processing affects the RWF beyond the transmitter and receiver effects captured in the conventional RWF formulation.

In this paper, a method is introduced to calculate the RWF arising from the processing of echo samples along the range-time dimension. It uses the following two elements: 1) a pulse matrix, which is based on the transmitter pulse envelope and the receiver filter, and 2) a transformation matrix, which is determined by the type of range-time processing. The pulse matrix is simply a discrete time convolution matrix, which has been used previously in the context of weather radar signal processing (e.g., Yu et al. 2006; Li et al. 2009); in this work, we employ it for the calculation of the RWF. The approach described herein combines both the pulse matrix and a transformation matrix capturing all three major contributors to the RWF—transmitter pulse envelope, receiver filter, and range-time signal processing.

The rest of this paper is structured as follows. Section 2 presents the basic method for computing the RWF, including information on how to construct the pulse matrix, the range-time signal processing model, and examples of different range-time processing techniques (i.e., different transformation matrices). Section 3 uses the RWF calculation to examine the range resolution of several range-time processing techniques and the correlation between meteorological data from adjacent resolution volumes. Finally, the results are summarized, and some recommendations for applying this work are given.

2. The range-weighting function

In this section we derive a general formulation of the RWF that includes the effects of range-time signal processing.

a. Model description

As depicted in Fig. 1, assume that the scatterers illuminated by the transmitted pulse (as it propagates in the radial direction away from the radar) can be modeled as a linear array of independent ''scattering centers'' uniformly spaced in range. The spacing between adjacent scattering centers is large compared to the radar wavelength but small compared to the range extent of the transmitter pulse. In this model, each scattering center represents the combined echo contributions (weighted by the two-way antenna beam pattern in azimuth and elevation) from all scatterers in an elemental spherical shell of thickness $\Delta r = c\Delta\tau_s/2$, where c is the speed of light and $\Delta\tau_s$ is much smaller than the transmitter pulse width τ. Although an analysis using a continuous propagation medium would be more realistic (e.g., Zrnić and Doviak 1978), the approximation of discrete scattering centers is preferred because it leads to a closed-form expression of the RWF. We assume that baseband, discrete time in-phase and quadrature (I and Q) signals, herein referred to as time series data, are produced at a rate T_r^{-1} (the time series data rate). Using the time series data as reference, our model consists of two elements. The first element combines the effects of transmission and reception up to the generation of the time series data,[1] and the second element consists of the range-time signal processing that is applied to the time series data to produce meteorological variable estimates.

Assuming that scatterers in a spherical shell have random placement but are ''frozen'' during the short time they are illuminated by the transmitted pulse [i.e., the ''frozen scatterers'' assumption from appendix C in Doviak and Zrnić (1993)], the contributions from each

[1] The first element of the model includes all of the filters used in the generation of the time series data. However, the actual sampling can occur at baseband or at the IF. In the baseband case, the first element of the model would include analog filters only (e.g., an analog matched filter). In the IF case, where additional digital filtering is used to produce the baseband time series data, the first element of the model would include both analog and digital filters (e.g., an analog bandpass filter and a digital matched filter).

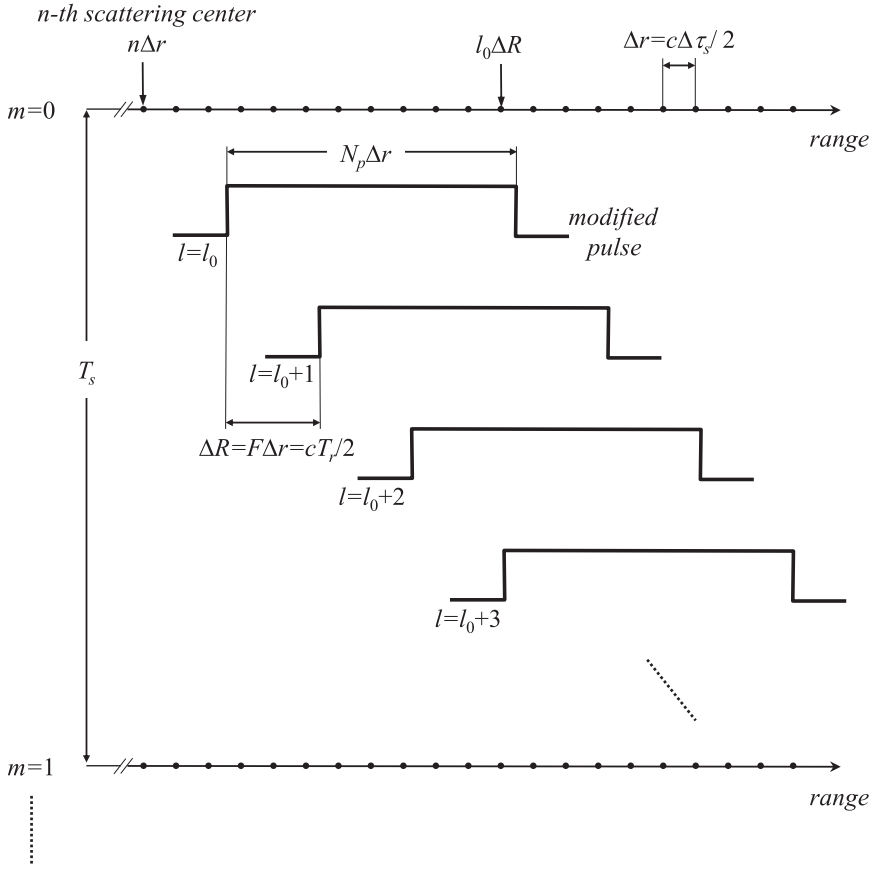

FIG. 1. Depiction of the modified pulse illuminating progressive sets of scattering centers as it propagates in the radial direction. Scattering centers are represented with dots along the range axis. A modified pulse of length N_p is shown at four range locations corresponding to four consecutive time series samples at times lT_r, where $l = l_0, l_0 + 1, l_0 + 2$, and $l_0 + 3$. The range-time sample spacing at the radar receiver is $T_r = F\Delta\tau_s$, where $\Delta\tau_s = 2\Delta r/c$, and Δr is the spacing between scattering centers. Meteorological data resolution volumes are typically spaced by $L\Delta R$, where $\Delta R = F\Delta r$ is the spacing between the resolution volumes corresponding to the time series data, and L is the range-oversampling factor. Samples along sample time are spaced by T_s (i.e., the pulse repetition time).

scattering center can be independently modeled as a baseband, stationary, complex Gaussian random process (section 4.1 in Doviak and Zrnić 1993). The random contributions from the nth scattering center along a radial are denoted by $S(n\Delta r, mT_s)$, where m is the discrete time index for the series of echo samples from sequential pulses associated with this particular scattering center. In other words, n indexes range (or range time) at Δr (or $\Delta\tau_s$) increments, and m indexes pulses (or sample time) at T_s (the pulse repetition time) increments. This is a valid simplification from the more accurate "dispersed pulse echo" analysis of Bucci and Urkowitz (1993); the reshuffling of scatterers in an elemental shell during the time it is illuminated by the transmitted pulse has no effect on the RWF, which depends on radar and signal processing parameters, not on properties of the medium.

1) TRANSMISSION AND RECEPTION MODELS

The nth scattering center would produce a baseband analog voltage δV_r at the receiver's front end of the same form as the envelope of the transmitter pulse e. That is, $\delta V_r(t, n\Delta r, mT_s) = S(n\Delta r, mT_s)e(t - n\Delta\tau_s)$, where t denotes continuous time. The baseband voltage δV_o after all receiver filters can be obtained by convolving the input waveform with the baseband-equivalent impulse response h of these receiver filters as

$$\begin{aligned}\delta V_o(\tau_s, n\Delta r, mT_s) &= S(n\Delta r, mT_s)\int_{-\infty}^{\infty} h(\tau_s - t)e(t - n\Delta\tau_s)\,dt \\ &= S(n\Delta r, mT_s)p(\tau_s - n\Delta\tau_s), \end{aligned} \quad (1)$$

where τ_s is a generic range time, and the "modified pulse" p is the envelope of the transmitted pulse smoothed by the receiver filter; thus, p includes the first two contributors to the RWF as described in the introduction. Assume that the time series sample spacing $T_r = F\Delta\tau_s$, where F is an integer. This creates time series data with corresponding resolution volumes spaced at $\Delta R = cT_r/2 = F\Delta r$. Whereas this sample spacing forces resolution volumes at multiples of the scattering-center spacing, this is not a limitation of the model because Δr and F can be chosen independently and arbitrarily to suit any particular time series data rate. With this sample spacing (i.e., $\tau_s = lT_r$), Eq. (1) becomes

$$\delta V_o(lT_r, n\Delta r, mT_s) = S(n\Delta r, mT_s)p[(lF - n)\Delta\tau_s]. \quad (2)$$

Finally, summing the contributions of all scattering centers at range time lT_r, the time series data V can be expressed as

$$V(lT_r, mT_s) = \sum_n S(n\Delta r, mT_s)p[(lF - n)\Delta\tau_s]. \quad (3)$$

In a well-designed radar, p must decay quickly away from its peak in order to achieve acceptable range localization of echoes. Hence, assume that $p(n\Delta\tau_s)$ is (or can be approximated to be) nonzero only for $0 \le n < N_p$, where $N_p\Delta\tau_s$ is the modified-pulse length in seconds (Fig. 1). Thus, for $lF > N_p$, the convolution with decimation in (3) becomes

$$V(l,m) = \sum_{n=lF-N_p+1}^{lF} S(n,m)p(lF - n), \quad (4)$$

where only the range- and sample-time indices are kept to simplify the notation. This equation clearly shows that the time series data at range time lT_r has contributions from a set of scattering centers ending with the lFth scattering center, which is consistent with the fact that returns from scatterers beyond $l\Delta R$ need more than lT_r seconds to arrive at the radar receiver.

Next, assume that N_v-by-M time series samples are needed to produce a set of meteorological variables for an arbitrary resolution volume and that these samples are indexed by $l_0 \le l < l_0 + N_v$ along range time and by $0 \le m < M$ along sample time, where l_0T_r is an arbitrary range time (Fig. 1). Note that depending on the type of range-time processing, the size, location, and spacing of the effective resolution volumes corresponding to the meteorological data may or may not match those of the resolution volumes inherent to the time series data. In fact, as will be shown later, the size and range location of the effective volumes for the meteorological data are determined by the associated RWF. The time series data needed to produce a set of meteorological variables can be obtained from (4) and written in matrix form as

$$\mathbf{V}_m = \mathbf{P}\mathbf{S}_m, \quad (5)$$

where $\mathbf{V}_m = [V(l_0, m), \cdots, V(l_0 + N_v - 1, m)]^{\mathrm{T}}$ is the vector of N_v time series data at sample time m, $\mathbf{S}_m = \{S[l_0F - N_p + 1, m], \cdots, S[l_0F + (N_v - 1)F, m]\}^{\mathrm{T}}$ is the vector of $N_s = N_p + (N_v - 1)F$ scattering-center voltages at sample time m, and $\mathbf{P}$ is the N_v-by-N_s modified-pulse convolution matrix (herein referred to as the pulse matrix). Superscript T denotes matrix transpose. The pulse matrix can be written as

$$\mathbf{P} = \begin{bmatrix} \overleftarrow{\mathbf{p}}_0 \\ \overleftarrow{\mathbf{p}}_F \\ \vdots \\ \overleftarrow{\mathbf{p}}_{(N_v-1)F} \end{bmatrix}, \quad (6)$$

where $\overleftarrow{\mathbf{p}}_0 = [p(N_p - 1), \cdots, p(1), p(0), 0, \cdots, 0]$, is the time-reversed, modified-pulse vector zero padded to N_s elements, and $\overleftarrow{\mathbf{p}}_n$ is $\overleftarrow{\mathbf{p}}_0$ circularly shifted to the right by n elements. That is, each row of $\mathbf{P}$ is formed by circularly shifting the previous row F elements to the right. Thus, multiplication with this pulse matrix results in a convolution with decimation, which captures the effects of the first two contributors to the RFW: the transmitted pulse envelope and the receiver filter.

2) RANGE-TIME SIGNAL PROCESSING MODEL

Time series data are processed to obtain autocovariance estimates for one resolution volume. The signal processing that occurs along the range-time dimension is, as mentioned previously, the third contributor to the RWF. A generalized model for the range-time processing involves two steps: transformation and estimation. Transformed signals at sample time m, $\mathbf{X}_m$, are obtained as

$$\mathbf{X}_m = \mathbf{T}\mathbf{V}_m, \quad (7)$$

where $\mathbf{T}$ is a complex-valued N_x-by-N_v transformation matrix. This transformation produces N_x samples, where N_x does not need to be equal to N_v. From these transformed samples, the lag-k autocovariance can be estimated as

$$\hat{R}(k) = \frac{1}{N_x(M - |k|)} \sum_{m=0}^{M-|k|-1} \mathbf{X}_m^{\mathrm{H}}\mathbf{D}\mathbf{X}_{m+k}, \quad (8)$$

where $\mathbf{D}$ is a complex-valued N_x-by-N_x autocovariance range-weighting matrix, and superscript H denotes conjugate transpose.

As mentioned in the introduction, the goal of this paper is to study the effects of range-time signal processing on

the RWF for weather radars. Although the presentation thus far has been general, focusing on time series data that are oversampled in range is useful for illustrating the effects of advanced range-time processing techniques such as range oversampling with pseudowhitening (Torres et al. 2004). A few cases are presented next that are typical when processing range-oversampled time series data. In this processing scenario, a digital matched filter, if needed, is implemented after generation of the time series data. This is unlike the conventional processing scenario for non-range-oversampled data in which the matched filter is implemented either in the analog domain or digitally in the intermediate frequency (IF) domain, before generation of the time series data. The reader should note that even though the model presented in this section can be used to study the effects of range-time signal processing on non-range-oversampled data, this processing scenario is normally limited to simpler techniques where the results are known or can be easily predicted from the conventional RWF formulation.

(i) Case A: Digital matched filtering without range averaging

This is the type of processing common to many weather radar systems with digital receivers, such as the National Weather Radar Testbed (NWRT) phased-array radar (PAR), and can be represented with the two-step model as

$$x_m = \mathbf{h}_{\mathrm{MF}}\mathbf{V}_m, \tag{9}$$

and

$$\hat{R}(k) = \frac{1}{M - |k|}\sum_{m=0}^{M-|k|-1} x_m^{\mathrm{H}} x_{m+k}. \tag{10}$$

Typically, k values (lags) of 0 and 1 are sufficient for the computation of reflectivity, Doppler velocity, and spectrum width estimates for a resolution volume. Here, $\mathbf{h}_{\mathrm{MF}}$ is the 1-by-L matched-filter vector,[2] where L is the range-oversampling factor ($L = 4$ on the NWRT PAR). It is easy to see that, for this case, $N_\nu = L$, $N_x = 1$ (i.e., the result after matched filtering is a scalar), $\mathbf{D} = [1]$ (a scalar), and $\mathbf{T} = \mathbf{h}_{\mathrm{MF}}$.

(ii) Case B: Whitening (or pseudowhitening) without range averaging

Range oversampling and whitening (or pseudowhitening) is a technique that can be used to improve the precision of spectral moment and polarimetric variable estimates on weather radars. Range oversampling provides more samples for the estimation of meteorological variables; these samples can be transformed (decorrelated) and efficiently used to reduce the variance of estimates and/or reduce the required observation (dwell) times (Torres and Zrnić 2003). This type of processing has been implemented on the NWRT PAR and it is the default mode of operation (Curtis and Torres 2011). Range oversampling and whitening (or pseudowhitening) can be modeled as follows:

$$\mathbf{X}_m = \mathbf{W}\mathbf{V}_m, \tag{11}$$

and

$$\hat{R}(k) = \frac{1}{L(M - |k|)}\sum_{m=0}^{M-|k|-1} \mathbf{X}_m^{\mathrm{H}}\mathbf{X}_{m+k}, \tag{12}$$

where L is the range-oversampling factor. For this case, $N_x = N_\nu = L$, $\mathbf{D} = \mathbf{I}$ (the L-by-L identity matrix), and $\mathbf{T} = \mathbf{W}$ (a range-oversampling transformation matrix). Here, $\mathbf{W}$ can be either the L-by-L whitening matrix obtained as the inverse square root of $\mathbf{C}_V$ (i.e., $\mathbf{W} = \mathbf{H}^{-1}$, where $\mathbf{C}_V = \mathbf{H}^*\mathbf{H}^{\mathrm{T}}$, and superscript asterisk (*) denotes complex conjugate) or a more general L-by-L pseudowhitening matrix, as described by Torres et al. (2004); $\mathbf{C}_V$ can be computed from the modified pulse as $\mathbf{C}_V = \|\mathbf{p}\|^{-2}\mathbf{P}^*\mathbf{P}^{\mathrm{T}}$, where $\mathbf{P}$ is the pulse matrix in (6), $\mathbf{p}$ is the modified-pulse vector $\mathbf{p} = [p(0), \ldots, p(N_p - 1)]$, and $\|\cdot\|$ is the vector-norm operator.

(iii) Case C: Digital matched filtering with range averaging

This is the type of range-time processing that entails averaging consecutive estimates along range for greater data precision at the expense of coarser range resolution. In this case, the matched filter is applied to nonoverlapping blocks of L-oversampled signals. For example, the 1-km legacy-resolution reflectivity data produced by the Weather Surveillance Radar-1988 Doppler (WSR-88D) is computed from the average of four signal power estimates spaced 250-m apart. This type of processing can be represented with the two-step model as

$$\mathbf{X}_m = \begin{bmatrix} \mathbf{h}_{\mathrm{MF}} & \mathbf{0}_L & \cdots & \mathbf{0}_L \\ \mathbf{0}_L & \mathbf{h}_{\mathrm{MF}} & \cdots & \mathbf{0}_L \\ \vdots & \vdots & \ddots & \vdots \\ \mathbf{0}_L & \mathbf{0}_L & \cdots & \mathbf{h}_{\mathrm{MF}} \end{bmatrix}\mathbf{V}_m, \tag{13}$$

and

$$\hat{R}(k) = \frac{1}{R(M - |k|)}\sum_{m=0}^{M-|k|-1} \mathbf{X}_m^{\mathrm{H}}\mathbf{X}_{m+k}, \tag{14}$$

[2] For deterministic signals, the classical matched filter is obtained as the time-reversed modified pulse. However, for stochastic signals with known covariance matrix, an optimal matched filter is obtained as the eigenvector corresponding to the maximum eigenvalue of the normalized range correlation matrix (Chiuppesi et al. 1980).

where R is the number of estimates in the range to average ($R = 4$ for the WSR-88D legacy-resolution reflectivity), and $\mathbf{0}_L$ denotes a row vector of L zeros. For this case, $N_\nu = RL$, $N_x = R$, $\mathbf{D}$ is the R-by-R identity matrix, and $\mathbf{T}$ is the R-by-RL transformation matrix with shifted matched-filter entries, as shown explicitly in (13).

(iv) Case D: Digital matched filtering with range interpolation

This type of processing can be useful when there is a point target (e.g., an aircraft) in an isolated resolution volume that obscures the meteorological data in the same volume. By assuming spatial uniformity of meteorological fields, data can be "rebuilt" using range interpolation of noncontaminated estimates. For example, the WSR-88D runs a strong-point clutter filter that detects and flags isolated resolution volumes with significant contamination by looking for abrupt discontinuities in a range profile of received signal powers. Autocovariances corresponding to flagged resolution volumes are obtained through linear interpolation (averaging) of neighboring noncontaminated values (section 3.2.1.2.2 in Unisys Corporation 1991). This type of processing can be represented with the two-step model as

$$\mathbf{X}_m = \begin{bmatrix} \mathbf{h}_{\mathrm{MF}} & \mathbf{0}_L & \mathbf{0}_L \\ \mathbf{0}_L & \mathbf{h}_{\mathrm{MF}} & \mathbf{0}_L \\ \mathbf{0}_L & \mathbf{0}_L & \mathbf{h}_{\mathrm{MF}} \end{bmatrix} \mathbf{V}_m, \tag{15}$$

and

$$\hat{R}(k) = \frac{1}{3(M - |k|)} \sum_{m=0}^{M-|k|-1} \mathbf{X}_m^H \begin{bmatrix} \frac{3}{2} & 0 & 0 \\ 0 & 0 & 0 \\ 0 & 0 & \frac{3}{2} \end{bmatrix} \mathbf{X}_{m+k}. \tag{16}$$

This case is similar to the previous one, except that $R = 3$ and $\mathbf{D}$ is a nontrivial matrix. Here, $N_\nu = 3L$, $N_x = 3$, and $\mathbf{T}$ is the 3-by-3L transformation matrix with shifted matched-filter entries in (15); $\mathbf{D}$ is the 3-by-3 matrix in (16), such that $\mathbf{D}/N_x$ results in the average of two autocorrelation estimates.

These cases cover a few common types of range-time processing and illustrate the generality of the proposed signal processing model. Other more complex approaches such as overlapped averaging in range, range filtering, and the efficient implementation of adaptive pseudowhitening (Curtis and Torres 2011) can also be represented with this model.

b. Range-weighting function computation

To compute the RWF using the proposed model, start by taking the expected value of (8). That is,

$$E[\hat{R}(k)] = \frac{1}{N_x(M - |k|)} \sum_{m=0}^{M-|k|-1} E(\mathbf{X}_m^{\mathrm{H}} \mathbf{D} \mathbf{X}_{m+k}). \tag{17}$$

The expected value inside the summation can be expanded using (7) and (5) as $E(\mathbf{S}_m^{\mathrm{H}} \mathbf{Q} \mathbf{S}_{m+k})$, where $\mathbf{Q} = \mathbf{P}^{\mathrm{H}} \mathbf{T}^{\mathrm{H}} \mathbf{D} \mathbf{T} \mathbf{P}$ is an N_s-by-N_s matrix. The triple product $\mathbf{S}_m^{\mathrm{H}} \mathbf{Q} \mathbf{S}_{m+k}$ can be written in terms of the individual elements as $\sum_{i=1}^{N_s} \sum_{j=1}^{N_s} [(\mathbf{S}_m)_i]^* (\mathbf{Q})_{ij} (\mathbf{S}_{m+k})_j$, where $(\mathbf{S}_m)_i$ is used to denote the ith element of vector $\mathbf{S}_m$, and $(\mathbf{Q})_{ij}$ is the (i, j) element of matrix $\mathbf{Q}$. Taking the expected value of the expanded product and pulling all constants outside the expectation operator,

$$E(\mathbf{S}_m^{\mathrm{H}} \mathbf{Q} \mathbf{S}_{m+k}) = \sum_{i=1}^{N_s} \sum_{j=1}^{N_s} (\mathbf{Q})_{ij} E[S^*(l_0 F - N_p + i, m) \times S(l_0 F - N_p + j, m + k)], \tag{18}$$

where the elements of $\mathbf{S}_m$ were explicitly identified. Note that the expectation inside the summation is the separable, two-dimensional autocovariance of scattering-center voltages $R_S^{(R)}(l_0 F - N_p + i, l_0 F - N_p + j) R_S^{(S)}(k)$, where superscripts (R) and (S) denote range- and sample-time autocovariances, respectively; and the scattering centers for the range-time autocovariance are explicitly identified because stationarity in range is not assumed. This two-dimensional autocovariance is zero for $i \neq j$ because the voltages from different scattering centers are statistically independent; that is, the scatterers they represent are contained in nonoverlapping elemental shells. It is now easy to show that (17) becomes

$$E[\hat{R}(k)] = \frac{1}{N_x} \sum_{n=1}^{N_s} (\mathbf{Q})_{nn} R_{S(l_0 F - N_p + n)}^{(S)}(k), \tag{19}$$

where the two-dimensional autocovariance was written as the sample-time autocovariance at lag k corresponding to the $(l_0 F - N_p + n)$-th scattering center. Equation (19) shows that sample-time autocovariance estimates at an arbitrary resolution volume consist of *weighted* contributions of sample-time autocovariances from scattering centers $l_0 F - N_p + 1$ to $l_0 F - N_p + N_s$. These weights, the diagonal entries of $\mathbf{Q}/N_x$, are in fact the RWF, herein denoted by w and defined as

$$w(n\Delta r) = \begin{cases} N_x^{-1} (\mathbf{P}^{\mathrm{H}} \mathbf{T}^{\mathrm{H}} \mathbf{D} \mathbf{T} \mathbf{P})_{nn} & l_0 F - N_p < n \leq l_0 F + (N_\nu - 1) F \\ 0 & \text{otherwise} \end{cases}. \tag{20}$$

Equation (20) provides the functional form of the RWF but does not provide explicit range localization. In other words, the range to be assigned to meteorological variables computed from the set of N_v time series data samples beginning at time $l_0 T_r$ is not obvious. However, the support of function w is the interval defined by $\Delta r(l_0 F - N_p + 1)$ and $\Delta r[l_0 F + (N_v - 1)F]$, so it seems logical that meteorological data be assigned to the range location corresponding to the middle point of this interval; that is,

$$r_0 = \left[l_0 F + \frac{(N_v - 1)F - N_p + 1}{2} \right] \Delta r. \qquad (21)$$

Another common way to assign range location is by considering the maximum of w; however, this definition does not work well for all types of range-time processing, such as those that produce multimodal RWFs. Still, for any of these range assignments to be valid, all of the scattering centers located in the support of the RWF must exhibit the same statistical properties in range (i.e., range stationarity). If this does not hold, as in the case of reflectivity gradients, then the range assignment must be corrected as described by Mueller (1977) or Johnston et al. (2002).

The computation of the RWF using (20) requires the pulse matrix **P**, the transformation matrix **T**, and the autocovariance range-weighting matrix **D**. Both **T** and **D** are directly determined from the specific range-time signal processing technique. In contrast, **P** depends on the modified pulse, which has to be measured. Measuring the modified pulse on actual radar systems can be done using two methods. The preferred method involves injecting a replica of the transmitter pulse into the receiver's front end and sampling it at the required rate $(\Delta\tau_s)^{-1}$. However, this may not be feasible in every radar system. A more practical method consists of capturing returns from a stationary point target (i.e., an isolated scattering object of size much smaller than the resolution volume, such as a tower) under clear-air conditions at the maximum available sampling rate. If this sampling is not fast enough, then a method is needed to obtain the modified pulse with the desired sample spacing of $\Delta\tau_s$. For this work, the NWRT PAR modified pulse was approximated using a coarsely sampled pulse measured from a tower. This pulse was then interpolated to a finer sampling grid ($\Delta\tau_s$) using cubic splines as shown in Fig. 2. Alternatively, the coarsely sampled modified pulse could be used directly. This would be equivalent to having coarsely spaced scattering centers ($F = 1$ in the most extreme case), which would not satisfy the condition that the scattering-center spacing is much smaller than the range extent of the transmitter pulse. Still, this approach could be useful to obtain the rough shape of the RWF directly from the measured data.

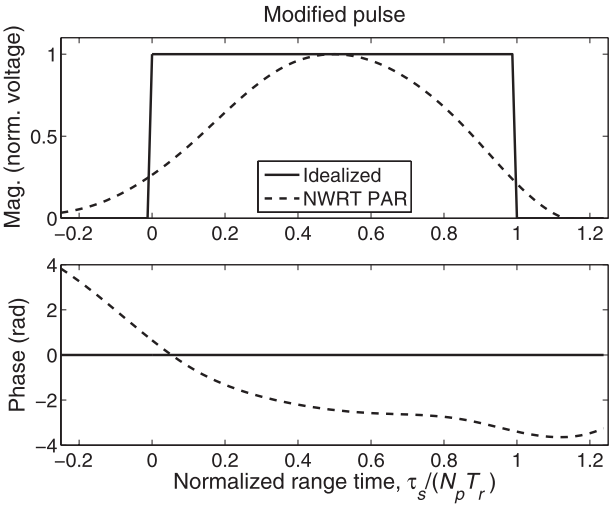

FIG. 2. (top) Magnitude and (bottom) phase of the idealized and NWRT PAR modified pulses as a function of normalized range time.

Figure 3 shows the normalized RWFs corresponding to the previously introduced cases with the specific signal-processing model parameters listed in Table 1. The RWFs are plotted as a function of range relative to their center or assigned range location r_0 (i.e., zero corresponds to r_0). Range values are plotted in $L\Delta R$ units because this is the typical spacing of meteorological data resolution volumes. For all cases, $F = 20$ (i.e., $T_r = 20\Delta\tau_s$) and the range-oversampling factor is $L = 4$. The cases depicted in the top panel correspond to the idealized case of a rectangular transmitter pulse envelope and a noiseless receiver having a receiver filter with very large bandwidth $B_6 \gg \tau^{-1}$ [recall that this is the bandwidth prior to any range-time processing, such as digital matched filtering (DMF)]. The length of the idealized modified pulse is $4T_r$. The cases in the middle and bottom panels correspond to the modified pulse of the NWRT PAR, which is more realistic with a length of $6T_r$. Both modified pulses are shown in Fig. 2. Note that the NWRT PAR modified pulse has a nontrivial phase, which can have a significant effect on the shape and symmetry of the RWF as discussed next.

For cases A and B with an idealized modified pulse, the depicted RWFs sampled at $\Delta\tau_s$ intervals are piecewise constant on $F\Delta\tau_s$ intervals. This occurs because the signal processing acts on samples spaced by $T_r = F\Delta\tau_s$, and the idealized modified pulse is constant over the time series sample spacing T_r. The RWFs vary from peaky to almost flat as the processing changes from a matched filter to whitening by stepping through varying degrees of pseudowhitening using a ''sharpening

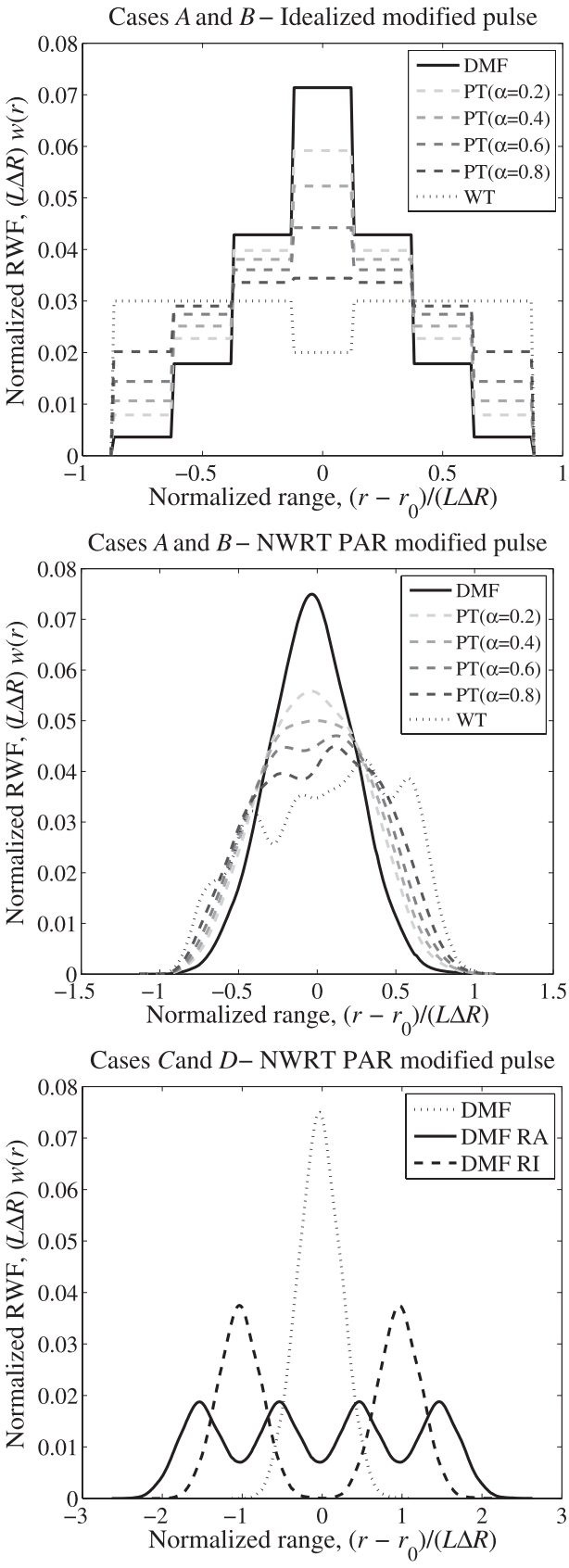

TABLE 1. Signal processing model parameters for the cases illustrated in Fig. 3. Matrix $\mathbf{T}$ is the N_x-by-N_ν transformation matrix, where N_ν and N_x are the number of raw and transformed range-time time series samples, respectively, and $\mathbf{D}$ is the N_x-by-N_x autocovariance range-weighting matrix. For these cases, $F = 20$ and $L = 4$; $\mathbf{I}$ is the identity matrix, $\mathbf{h}_{MF}$ is the matched-filter vector, $\mathbf{W}_{WH}$ is the whitening-transformation matrix, and $\mathbf{W}_{SH}$ is the pseudowhitening transformation matrix based on a sharpening filter with parameter α; and diag($\boldsymbol{a}_1$, $\boldsymbol{a}_2$, . . . , $\boldsymbol{a}_n$) defines a block (or partitioned) matrix containing vectors $\boldsymbol{a}_1, \boldsymbol{a}_2, \ldots, \boldsymbol{a}_n$ on the diagonal and zeros elsewhere.

Case	N_ν	N_x	**T**	**D**
A	4	1	$\mathbf{h}_{MF}$	1
B	4	4	$\mathbf{W}_{WH}$ and $\mathbf{W}_{SH}$ (α = 0.2, 0.4, 0.6, 0.8)	$\mathbf{I}$
C	16	4	diag($\mathbf{h}_{MF}$, $\mathbf{h}_{MF}$, $\mathbf{h}_{MF}$, $\mathbf{h}_{MF}$)	$\mathbf{I}$
D	12	3	diag($\mathbf{h}_{MF}$, $\mathbf{h}_{MF}$, $\mathbf{h}_{MF}$)	diag(3/2, 0, 3/2)

filter'' with parameter α, where $0 \le \alpha \le 1$ (Torres et al. 2004). The degree of pseudowhitening is related to the variance of meteorological variable estimates obtained from the corresponding transformation. If α is close to zero, then pseudowhitening approaches the performance of matched filtering. As α increases, the variance of estimates (at high SNR) decreases until $\alpha = 1$, which corresponds to whitening. Thus, as α goes from 0 to 1, the variance of estimates decreases but the corresponding RWFs become broader. For the NWRT PAR modified pulse, the RWFs exhibit a similar trend, but they become more asymmetric about r_0 because of the nontrivial phase and asymmetry of the modified pulse. Unlike the RWFs from the idealized modified pulse, the RWFs from the NWRT PAR modified pulse are not piecewise constant because this modified pulse is *not* piecewise constant over the time series sample spacing ($F\Delta\tau_s$).

The RWFs corresponding to processing cases C and D are examples of multimodal RWFs, which are based on the digital-matched filter RWF (case A). As expected, for processing that involves averaging consecutive

←

FIG. 3. Normalized RWFs corresponding to the cases in Table 1 as a function of normalized range (relative to r_0, in $L\Delta R$ units). The RWF for (top) A and (middle) B cases; i.e., DMF, WT, and pseudowhitening transformation (PT) based on a ''sharpening filter'' with parameter α = 0.2, 0.4, 0.6, and 0.8. (bottom) The RWF for cases C and D; i.e., a DMF with range averaging (RA), and a DMF with range interpolation (RI). Case A (DMF) is also included as a reference. The top panel corresponds to the idealized modified pulse of length $4T_r$; i.e., a rectangular transmitter pulse envelope and a receiver filter with a large bandwidth $B_6 \gg \tau^{-1}$. The middle and bottom panels correspond to the modified pulse of the NWRT PAR of length $6T_r$. All RWFs are normalized for unit area and plotted in $(L\Delta R)^{-1}$ units.

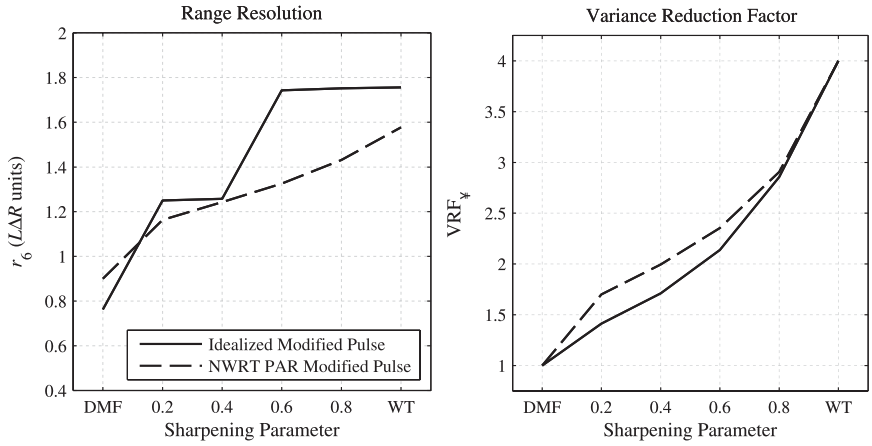

FIG. 4. (left) Range resolution (r_6) and (right) variance reduction factor (VRF_∞) for cases A and B, including a DMF, a WT, and pseudowhitening transformations with varying sharpening parameter α. An idealized modified pulse (solid line) and the modified pulse of the NWRT PAR (dashed line) are shown.

meteorological variable estimates in range (case C), the RWF consists of R shifted ''replicas'' of the RWF prior to averaging. On the other hand, for processing that involves range interpolation of meteorological variable estimates (case D), it is evident that one or more of the central scattering centers do not contribute at all to the meteorological data. In all these cases, r_0 corresponds to the middle of the RWF, as defined in (21).

Although the shape of the RWF conveys important information, a more concise way to characterize and compare the RWFs for different types of processing is by looking at the corresponding range resolution. The RWF also determines the correlation of meteorological data in range. Both of these are addressed in the next section.

3. Range resolution and range correlation

The range resolution is directly related to the size of the radar resolution volume. For point targets, the range resolution measures the ability of the radar to distinguish two targets along a given direction. For weather radars, distributed meteorological scatterers are the targets of interest, but the range resolution is still important for observing finescale phenomena, such as tornado vortices. For example, Brown et al. (2005) showed that many signatures (e.g., gust fronts, hook echoes, bounded weak echo regions) could be identified at farther ranges by using meteorological data with finer range and angular resolution.

As shown in the previous section, processing along the range-time dimension affects the RWF, and this has the potential to change the radar range resolution. In some cases, range-time signal processing can be used to improve the range resolution, for example, pulse compression (Mudukutore et al. 1998) and the Resolution Enhancement Technique using Range Oversampling (RETRO; Yu et al. 2006). In other cases, range resolution can be traded for meteorological data fields with improved precision, for example, range-oversampling techniques (Torres and Zrnić 2003; Torres et al. 2004) and conventional range averaging of meteorological variable estimates.

The standard way to define the range resolution for weather radars is in terms of the resolution volume. Doviak and Zrnić (1993) define the resolution volume as the volume circumscribed by the 6-dB contour of the product of the two-way antenna beam pattern and the RWF. The range resolution, denoted by r_6, is defined as the 6-dB width of the RWF. In this case, the 6-dB decrease is measured from the ends of the RWF with respect to the maximum value. This approach removes ambiguity when computing the width of multimodal RWFs (e.g., case C in Fig. 3).

Figure 4 shows the 6-dB (r_6) widths and variance reduction factor at high SNR (VRF_∞) for cases A and B (Fig. 3) using the idealized and NWRT PAR modified pulses (Fig. 2). The widths are given in $L\Delta R$ units, which correspond to the meteorological data resolution volume spacing. VRF_∞ is defined as the ratio of the variance of estimates from matched filtering to the variance from pseudowhitening, both at high SNR. For the idealized pulse, the width is approximately $0.76L\Delta R$ for the digital matched filter and VRF_∞ is 1. As expected, both VRF_∞ and the range width increase (i.e., the range resolution becomes coarser) as the RWF becomes less peaky; the width increases to about $1.76L\Delta R$ for range oversampling with a whitening transformation and VRF_∞

goes to L (in this case, $L = 4$). There are jumps in the range resolution for the idealized pulse because of the discontinuities in the piecewise-constant RWF. For the more realistic NWRT PAR modified pulse, the same effects can be seen—VRF_∞ goes from 1 to L, but the widths are slightly reduced (except for the matched filter) because of the larger roll-off factor. The widths range from $0.9L\Delta R$ for the digital matched filter to $1.58L\Delta R$ for whitening. In the idealized case, the range width increases by a factor of 2.3 when using whitening compared to digital matched filtering, while it only increases by 1.75 for the NWRT PAR modified pulse. In both cases, the range width for whitening increases to a value greater than the resolution volume spacing, which shows that there is more overlap in range than usual. The effect of this overlap will be quantified later by examining the range correlation.

For case D with the NWRT PAR modified pulse, the width is calculated from the ends so $r_6 \approx 2.9L\Delta R$. This is consistent with computing the meteorological variables by interpolating nonobscured data from resolution volumes on either side of the contaminated resolution volume. For case C, $r_6 \approx 3.9L\Delta R$; that is, the width matches what we would expect from averaging four matched-filter samples.

In addition to computing the range resolution, the RWF can be used to calculate the correlation between meteorological data from two adjacent resolution volumes. The correlation coefficient is computed by summing the products of the RWF values that overlap and then scaling so that the value is one for completely overlapping RWFs (i.e., zero range spacing). The correlation coefficient between data from adjacent resolution volumes is shown in Fig. 5 for both the idealized modified pulse and the more realistic modified pulse measured on the NWRT PAR. As in Fig. 4, the data correspond to cases A and B. The correlation coefficient in the idealized case ranges from about 0.07 for digital matched-filter processing (i.e., almost uncorrelated data) to 0.47 for range oversampling and whitening. For the NWRT PAR modified pulse, the correlation coefficient is approximately 0.03 for matched-filtered processing and 0.32 for whitening. This clearly quantifies the expected increase in correlation between the two types of processing. Another way to use the correlation is to examine how far apart resolution volumes for data obtained with range oversampling and whitening would need to be to have the same correlation coefficient as adjacent resolution volumes with matched-filter data. For the idealized case, the meteorological data resolution volume spacing would need to increase by a factor of about 1.65 to have the same correlation as the digital matched-filter processing and by a factor of about 1.5 for the case using the NWRT PAR modified pulse.

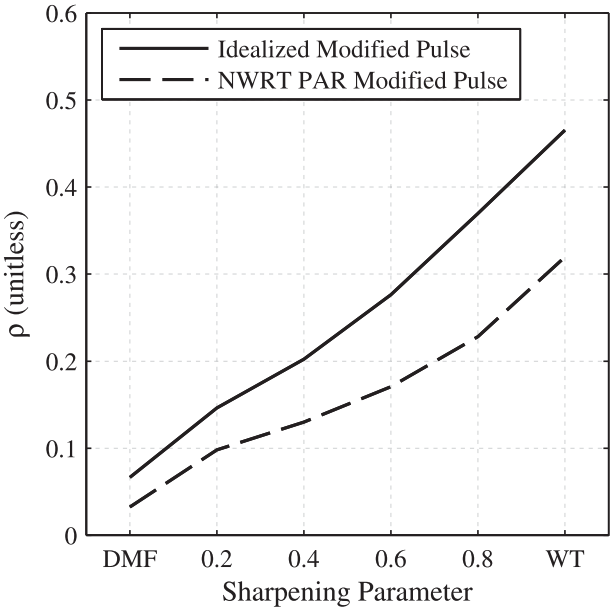

FIG. 5. Correlation coefficient (ρ) between meteorological data from adjacent resolution volumes with range spacing of $L\Delta R$ for cases A and B including a DMF, a WT, and pseudowhitening transformations with varying sharpening parameter α. An idealized modified pulse (solid line) and the modified pulse of the NWRT PAR (dashed line) are shown.

In summary, the RWF is a tool that can be used to examine the effects of different types of range-time processing. In this section, we used it to study the effects of range-time processing on both the range resolution and range correlation.

4. Conclusions

We derived a new formulation of the range-weighting function (RWF) for weather radars that includes the effects of range-time signal processing. Traditionally, the RWF has been defined solely in terms of the transmitter pulse envelope and the receiver filter impulse response. However, we showed that the effective RWF also depends on the signal processing techniques that operate along the range-time dimension (e.g., range oversampling, range averaging, and range interpolation). This contributor to the RWF has gained significance in recent years as advanced range-time processing techniques have become feasible for real-time implementation on modern radar systems.

After deriving the RWF based on a general signal processing model, typical sampling and signal processing schemes from operational weather radars were used to illustrate a variety of possible RWFs. Not only is precise

knowledge of the RWF critical in the assignment of range to meteorological data, but it is also required for estimating biases from spatial gradients of meteorological fields. The RWF is also essential for measuring the range resolution and range correlation of meteorological data, which are important characteristics of radar systems.

This new formulation will be useful for characterizing modern radar systems that operate on range-oversampled signals (either by employing a digital matched filter or by exploiting more advanced processing techniques) and evaluating the impact that signal processing has on the performance of algorithms that rely on spatial features of meteorological data.

Acknowledgments. The authors thank Dick Doviak, Dusan Zrnić, Igor Ivić, and three anonymous reviewers for providing very useful comments that helped improve the manuscript. Funding was provided by NOAA/Office of Oceanic and Atmospheric Research under NOAA–University of Oklahoma Cooperative Agreement NA17RJ1227, U.S. Department of Commerce.

REFERENCES

Bringi, V. N., and V. Chandrasekar, 2001: *Polarimetric Doppler Weather Radar: Principles and Applications*. Cambridge University Press, 636 pp.

Brown, R. A., B. A. Flickinger, E. Forren, D. M. Schultz, D. Sirmans, P. L. Spencer, V. T. Wood, and C. L. Ziegler, 2005: Improved detection of severe storms using experimental fine-resolution WSR-88D measurements. *Wea. Forecasting,* **20,** 3–14.

Bucci, N. J., and H. Urkowitz, 1993: Testing of Doppler tolerant range sidelobe suppression in pulse compression meteorological radar. *Proc. IEEE National Radar Conf.,* Boston, MA, IEEE, 206–211.

Capsoni, C., and M. D'Amico, 1998: A physically based radar simulator. *J. Atmos. Oceanic Technol.,* **15,** 593–598.

Cheong, B. L., M. W. Hoffman, and R. D. Palmer, 2004: Efficient atmospheric simulation for high-resolution radar imaging applications. *J. Atmos. Oceanic Technol.,* **21,** 374–378.

——, R. D. Palmer, and M. Xue, 2008: A time series weather radar simulator based on high-resolution atmospheric models. *J. Atmos. Oceanic Technol.,* **25,** 230–243.

Chiuppesi, F., G. Galati, and P. Lombardi, 1980: Optimisation of rejection filters. *IEE Proc. F Commun. Radar and Signal Process.,* **127,** 354–360.

Curtis, C., and S. Torres, 2011: Adaptive range oversampling to achieve faster scanning on the National Weather Radar Testbed phased array radar. *J. Atmos. Oceanic Technol.,* **28,** 1581–1597.

Doviak, R. J., and D. S. Zrnić, 1993: *Doppler Radar and Weather Observations.* 2d ed. Academic Press, 562 pp.

Johnston, P. E., L. M. Hartten, C. H. Love, D. A. Carter, and K. S. Gage, 2002: Range errors in wind profiling caused by strong reflectivity gradients. *J. Atmos. Oceanic Technol.,* **19,** 934–953.

Li, X., J. He, J. Wang, and Z. Si, 2009: A robust capon method to improve weather radar range resolution using oversampling. *Proc. 2009 Int. Conf. on Information Engineering and Computer Science,* Wuhan, China, IEEE, 1–4.

Mudukutore, A. S., V. Chandrasekar, and R. J. Keeler, 1998: Pulse compression for weather radars. *IEEE Trans. Geosci. Remote Sens.,* **36,** 125–142.

Mueller, E. A., 1977: Statistics of high radar reflectivity gradients. *J. Appl. Meteor.,* **16,** 511–513.

Torres, S., and D. Zrnić, 2003: Whitening in range to improve weather radar spectral moment estimates. Part I: Formulation and simulation. *J. Atmos. Oceanic Technol.,* **20,** 1433–1448.

——, and C. D. Curtis, 2006: Design considerations for improved tornado detection using super-resolution data on the NEXRAD network. Preprints, *Fourth European Conf. on Radar Meteorology and Hydrology (ERAD),* Barcelona, Spain, ERAD, 92–95.

——, ——, and J. R. Cruz, 2004: Pseudowhitening of weather radar signals to improve spectral moment and polarimetric variable estimates at low signal-to-noise. *IEEE Trans. Geosci. Remote Sens.,* **42,** 941–949.

Unisys Corporation, 1991: Computer program development specification for signal processing program (B5, CPCI 02), DV1208261F. [Available from WSR-88D Radar Operations Center, 1200 Westheimer Dr., Norman, OK 73069.]

Wood, V. T., and R. A. Brown, 1997: Effects of radar sampling on single-Doppler velocity signatures of mesocyclones and tornadoes. *Wea. Forecasting,* **12,** 928–938.

Yu, T.-Y., G. Zhang, A. Chalamalasetti, R. Doviak, and D. Zrnić, 2006: Resolution enhancement technique using range oversampling. *J. Atmos. Oceanic Technol.,* **23,** 228–240.

Zrnić, D. S., and R. J. Doviak, 1978: Matched filter criteria and range weighting for weather radar. *IEEE Trans. Aerosp. Electron. Syst.,* **AEC-14,** 925–930.